LBL--14641

DE82 020267

LBL-14641

BEHAVIOR OF NUCLEI AT HIGH ANGULAR MOMENTUM

F.S. Stephens

Nuclear Science Division, Lawrence Berkeley Laboratory
University of California, Berkeley, CA 94720

This work was supported by the Director, Office of Energy Research, Division of Nuclear Physics of the Office of High Energy and Nuclear Physics of the U.S. Department of Energy under Contract DE-AC03-76SF00098.

LBL-14641

BEHAVIOR OF NUCLEI AT HIGH ANGULAR MOMENTUM

F.S. Stephens
Nuclear Science Division, Lawrence Berkeley Laboratory
University of California, Berkeley, CA 94720

Abstract

The present report begins with a brief overview of nuclear shapes and level structures at high-spin values. The new spectroscopy associated with angular-momentum alignments is described, and some of the exciting possibilities of this spectroscopy are explored. Nuclear moments of inertia are discussed and a somewhat different one is defined, together with a method for measuring it and some early results. Finally a few comments on the future prospects for high-spin physics are offered.

1. Introduction

I would like to do two things in this report. First, I want to try to give an overview on the field of high-spin physics, in the hope that for some it might help tie together the many varied and interesting papers we are going to hear. And second, I want to try to clarify somewhat the ideas we have about moments of inertia in nuclei. Out of this "clarification" will come a definition for a moment of inertia that is slightly different from those presently used, together with a new method for measuring it. The study of high spin states in nuclei has developed rapidly in the last few years and is now in a fortunate position where there is both a diversity of interesting aspects and yet a reasonably simple overall understanding.

2. Nuclear Shapes

One of the most important factors in determining the physics of high-spin states is simply the rotational behavior of rigid classical objects. In Fig. 1 the moment of inertia of such an object is compared with that of a rigid sphere (solid lines) for a variety of shapes and rotational axes. The shape and axis is defined by γ, which varies from -120° to 60° as the object varies from a prolate shape rotating about its symmetry axis, through oblate and prolate shapes rotating about axes perpendicular to the symmetry axis, to an oblate shape rotating

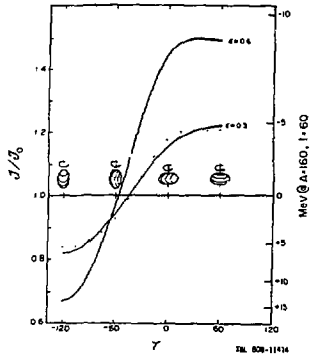

Fig. 1. The ratio of the moment of inertia of a rigid ellipsoid to that of a rigid sphere vs the shape parameter γ for two values of the deformation $\varepsilon = 0.3$ and $\varepsilon = 0.6$. The right-hand scale gives the difference in rotational energy in MeV for a nucleus with A = 160 and I = 60. The dots give the ratios for the total liquid-drop energy (rotation + surface + Coulomb) of the nucleus.

about its symmetry axis. The deformation is given in terms of a quantity ε, which is to lowest order just $\Delta R/R$. Values of ε around 0.3 are typical for the familiar deformed rare-earth and actinide nuclei. The largest moments of inertia, and therefore the lowest rotational energies, occur for the range of shapes between $\gamma = 0°$ and 60°. The very largest moment of inertia is for $\gamma = 60°$, an oblate shape rotating around its symmetry axis, and it is for this reason the earth has such a shape. The full liquid-drop model (LDM) treatment of a rotating nucleus[1] includes volume, surface, and Coulomb energies, in addition to these classical rotor considerations, and is shown by the dots in Fig. 1. It is apparent that there is no strong shape preference in these additional LDM terms, so that simple classical mechanics determine the liquid-drop shapes. This is important, since the liquid-drop model is our best guide to such macroscopic nuclear properties and is even the limit to which some of the microscopic models are normalized.

In order to see how significant these classical shape effects are, one must choose a mass and spin, and for A = 160 and I = 60 $\hbar$, an energy scale is given on the right side of Fig. 1. The variation for $\varepsilon = 0.3$ of about 10 MeV is larger than typical shell effects ($\sim$3 MeV) so that for this spin the effects considered here should be dominant. The rotational energy varies as I^2 so that, for 30 $\hbar$, shell effects and these

classical shape effects should be about equivalent, and below ∿20 ħ the shell effects will dominate. The arguments made here would seem to apply only for collective nuclear rotations, and even then only if the nuclear moment of inertia has the rigid body value, neither of which is obviously the case. In fact, however, most people do believe that rotating nuclei at high spins will, on average, have the rigid-body moment of inertia, and this has been shown to be the case for an anisotropic harmonic oscillator potential and independent particle motion[2]. The smaller moments of inertia observed at low spins are due largely to the pairing correlations, which should be quenched above ∿30 ħ. Furthermore, even in noncollective cases, it has been shown (for a Fermi gas) that the trajectory of lowest levels follows that given by rotating the appropriately shaped rigid body[3]. Thus, these very simple arguments should be valid and shapes in the γ = 0-60° range should dominate at high spin, i.e., above ∿30 ħ in the A = 160 region.

These expectations as to nuclear shapes are borne out by the microscopic calculations that have now been made for most nuclei using several different models. This is shown[4] in Fig. 2 where the left side shows the ß-γ plane divided

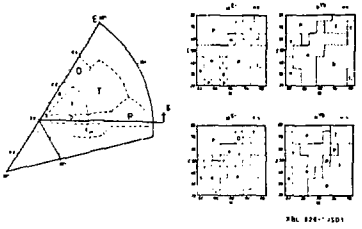

Fig. 2. The left side identifies various regions in a ß-γ plot with appropriate symbols. The right side shows the shape (by symbol) calculated to be lowest in energy for E_γ and Yb nuclei as a function of spin and neutron number. Dashed boundaries indicate barriers less than 1 MeV between the regions; whereas, solid boundaries correspond to greater than 1 MeV barriers. Solutions for two potentials are shown--modified oscillator and Woods-Saxon. From ref. 4.

arbitrarily into regions of large or small deformation having prolate, triaxial, or oblate shapes. On the right side, the lowest energy shapes of some Er and Yb nuclei are indicated as a function of spin and neutron number for two different potentials--the modified oscillator (Nilsson) and the Woods-Saxon. Perhaps most apparent in this figure is that it is necessary to label essentially only the γ = 0-60° range. No other shapes are calculated to occur (except for a small region of γ slightly less than 0°, t_{-}). Further, the two different models agree remarkably well in overall features, although there are some differences in detail. The dashed lines between different shape regions indicate a barrier of less than 1 MeV, corresponding most likely to a gradual transition between shapes. Almost all the shape changes with increasing spin in this whole region (in both models) are predicted to be of this type. Discontinuous shape changes are predicted only for the large prolate shapes (super-deformed) that are calculated to occur at very high spins and moderate to low neutron numbers. There are a great variety of shapes predicted in Fig. 2, especially in the N = 86-90 region, and there is much interest right now in looking for these shapes in the nuclei of this region.

3. Level Structures

A general question arises as to how one can recognize these shapes experimentally. That is, what kind of nuclear structure is expected for shapes in this γ = 0-60° region. It has been recognized since 1952 that a deformed nucleus can rotate collectively around an axis perpendicular to the symmetry axis[5]. The prolate γ = 0° shape is of this type and essentially all the rotational nuclei known have γ-values equal to or near 0°. On the other hand, a nucleus cannot rotate collectively around a symmetry axis; those degrees of freedom are contained in the single-particle motion. Thus the γ = 60° oblate nuclei do not have collective rotation, but build up their angular momentum by aligning along a common axis the contribution of various single particles. The kind of structure associated with the triaxial nuclear shapes between γ = 0° and 60° has been elucidated recently--since the first clues to this were found in the back-bending phenomenon discovered[6] in 1971. The situation is depicted in Fig. 3. For exactly axially symmetric shapes (upper

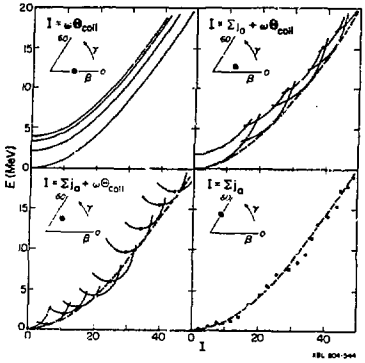

Fig. 3. Schematic excitation energy vs spin plots for various relative amounts of collective angular momentum and single-particle rotation-aligned angular momentum. Bandhead (pure single-particle) energies are shown in the lower two panels. The solid curves correspond to real bands, whereas the dashed curve is the envelope of the real bands.

left) only collective rotation is possible, and different configurations give rise to bands that extend over broad regions of spin. In fact, what is observed to happen is indicated at the upper right, where bands with different configuration have different amounts of single-particle angular momentum aligned with the rotation axis and thereby give rise to slightly nonaxial shapes and a pattern of crossing bands. Sequences with spins up to ~40 ħ have now been observed with three successive alignments (band crossings) that provide about half the total angular momentum of the nucleus. As γ moves closer to 60° (lower left) the proportion of single-particle to collective angular momentum becomes larger, and the rotational bands become less collective with smaller moments of inertia. This situation probably occurs in nuclei like ^{154}Er in the I = 30-40ħ region[7] and in ^{154}Dy near[8] I = 40 ħ, but is certainly the least documented of the regions of Fig. 3. Finally, at the lower right of Fig. 3, the collective motion is very weak or entirely absent, and we now suspect many nuclei in the N = 82, Z = 64 region are of this type. So far only ^{147}Gd has quadrupole moments measured to indicate a nonspherical shape[9], but nuclei like ^{152}Dy and ^{150}Gd are very likely of this type. It is not so easy to distinguish these spectra from those of nuclei with spherical shapes, but quadrupole moments can do this, and there may be additional features of the spectra that can help (the rotation about the perpendicular axes?). In any case, the main point

here is that there are characteristic spectra associated with the shapes between $\gamma = 0°$ and 60°, and these are rather easy to distinguish experimentally. Furthermore, the range of spectral types is (or can be) continuous, as it must be since γ is (or can be) continuous.

It should be recognized that there is no simple path through Fig. 3 along which nuclei evolve with increasing spin. It was clear in Fig. 1 that the $\gamma = 0$ to 60° region was quite flat in the LDM limit, so that shell effects determine just where in this range a given nucleus will be. Some nuclei like ^{154}Dy recently discussed by Khoo[8] seem to progress from upper right to lower left and probably on to lower right as the spin goes from 20 to 40 $\hbar$. However, its neighbor ^{152}Dy shifts from lower-right-type behavior in the 20-40$\hbar$ range to some type (as yet not well specified) of collective behavior at higher spins[10]. The shell effects determine such specific behaviors. However, one generalization we can make that will be interesting for the highest spin regions is that more single-particle angular momentum generally indicates behavior closer to the $\gamma = 60°$ limit, and conversely a larger fraction of collective angular momentum usually means a shift towards $\gamma = 0°$.

4. The New Spectroscopy

One of the important things we have learned about studying nuclei at high spins is the importance of using the rotational frequency, ω, as a parameter rather than the angular momentum, I. The reason for this is that I contains comparable contributions from two sources--collective rotation and single particle alignment. Thus, it is not a good variable to study either behavior. On the other hand, ω is related only to the collective rotation, and thus is a variable that provides a possibility to separate these two aspects of high angular momentum states. Furthermore, although I is the quantized quantity, ω is even more readily accessible experimentally. For all but the lowest spins, it is adequate to use $\omega = E_\gamma/2$, where E_γ is the collective rotational transition. There is really nothing more readily measured than these E_γ values. Thus our plots and analyses will generally be in terms of the angular frequency, ω.

A large amount of work has recently been done in studying detailed nuclear levels in the I = 0 to $\sim$30 $\hbar$ range. Our

understanding of nuclear behavior in this spin region has progressed enormously, and I want to give you some clue as to what to expect in such studies. A single level scheme, of ^{160}Yb, is shown in Fig. 4 on an energy vs spin plot[11]. The various bands are connected and one sees in addition to two band crossings along the yrast line, a very large number (shown or implied) above it. The organization of such information is now rather far advanced, and I want to outline that for you.

The first step of reduction is shown in Fig. 5 where for ^{158}Er (very similar to ^{160}Yb) the properties of the yrast sequence are plotted[12] against ω. At the top the moment of inertia, $\mathcal{J}$ (defined here as I/ω or approximately as $2I/E_\gamma$), is shown, and two sizeable discontinuities (a backbend and an upbend) are clear. These are the band crossings I have been discussing, and it is now known that the first of these at $\hbar\omega \approx 0.25$ MeV corresponds to the alignment of two $i_{13/2}$ neutrons and the second at $\hbar\omega \approx 0.42$ MeV to an additional alignment of two $h_{11/2}$ neutrons. The middle curve shows I plotted against ω, and regions corresponding to three bands are rather

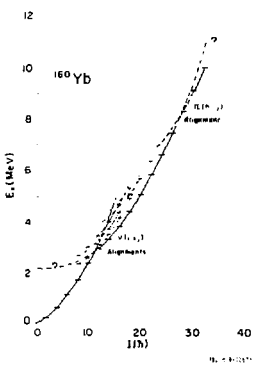

Fig. 4. Rotational band trajectories on an E vs I plot for the levels of ^{160}Yb. The observed levels are indicated by the horizontal marks. From ref. 11.

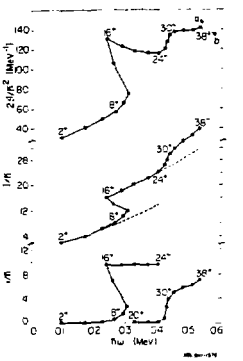

Fig. 5. Plots of the moment of inertia (top), spin (middle), and spin alignment (bottom) vs the rotational frequency for the yrast sequence in ^{158}Er. From ref. 12.

easily seen, the lower two of which have been extrapolated to higher frequencies (dashed lines). The increase in aligned angular momentum for each band change, i, can be estimated by subtracting the spin in the lower band from that in the upper at a given frequency. The assumption here is that the collective contributions to the two bands are the same at the same rotational frequency. The bottom curve shows the aligned angular momentum for each case, about 10 ħ for the $i_{13/2}$ neutrons and 5-6 ħ for the $h_{11/2}$ protons. Thus, associated with a band crossing, or alignment, are three quantities--a critical frequency for the crossing, ω_c; an aligned angular momentum, i, and an interaction between the bands, V, which determines how sharp the crossing is, i.e., a large backbend, an upbend, or a crossing so smoothed out it may be hard to tell there was any band crossing at all. Part of the new spectroscopy is the identification of observed band crossings with those calculated using these three measurable characteristics. This is, however, by no means the limit of this new game.

The next level of analysis can be visualized using Fig. 6. Here are shown[13] aligned angular momentum plots for three bands in ^{160}Yb and two in ^{161}Yb. The two alignments for the yrast sequency of ^{160}Yb are seen to be rather similar to those

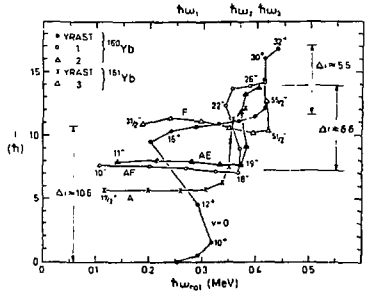

Fig. 6. Spin alignments vs rotational frequency for measured level sequences of ^{160}Yb and ^{161}Yb. The quasiparticle orbits assigned to be occupied in respective level sequences are denoted by A, AF, etc., while the quasiparticle vacuum is denoted by v = 0. The band crossing frequencies associated with the increment of spin alignments $\Delta i \approx 10.6$, 6.6, and 5.5 are indicated by ω_1, ω_2, and ω_3, respectively. From ref. 13.

of ^{158}Er, and give alignments, critical frequencies, and backbend shapes (interactions) that are quite comparable. The band labeled 3 (or F) in ^{161}Yb is presumably similar but is seen only for the upper of these two alignments. However, it is the intermediate three alignment curves that are of special interest. These all correspond to aligning the same particles--$i_{13/2}$ neutrons, but a different pair from that discussed above. The highest possible alignment for two $i_{13/2}$ neutrons along any axis is 13/2 + 11/2 = 12 ħ, and this pair aligned along the rotation axis is generally called "AB". For the three interme- diate cases in Fig. 6 the state "A" is blocked by a single particle and the remaining best alignment possible in the $i_{13/2}$ neutron shell is 11/2 + 9/2 = 10 ħ, called "BC". To lowest order this alignment ought to come at the same frequency in any band (configuration) in which it occurs. This is approximately true in Fig. 6, but not quite. In ^{161}Yb where only A is blocked, the crossing frequency is slightly lower than in the bands of ^{160}Yb where an additional level, E or F, is blocked. Thus in higher order the remaining configuration <u>does</u> affect the crossing frequency, and in this case it is thought to do so by changing the pairing correlations and thus the pairing gap. Systematic studies of these small shifts due to configuration have been made by Garrett, Herskind, and others[14] in Copenhagen and have led to te determination of pairing gaps for individual configuration (bands). Let me try to intrigue you with the comment that Bent Herskind will tell us on Friday how to learn about quadrupole pairing in nuclei from such studies. I believe it is very significant that we have a nuclear property--angular frequency--which we can vary for virtually any configuration in any nucleus and observe the resulting changes. This is indeed a new type of nuclear spectroscopy.

These alignments in nuclei are not really so different from what happens in some other areas of physics. If we turn around our perspective and think of a nucleus slowing down from a high initial spin obtained (for example) in a nuclear reaction, then the rotational frequency slowly decreases, producing an increase in the rotational period. This regular increase in period (slowing down) is sometimes interrupted by rather sizeable decreases. These correspond to internal rearrangements,

"nuclearquakes", and are just our alignment process. It is amusing to compare it with another type of quake--a "starquake". Neutron stars or "pulsars" also have regularly increasing periods that occasionally decrease suddenly. The slowing down of the nucleus ^{158}Er is compared with the pulsar Vela in Fig. 7. The behaviors are quite similar, though the percentage changes in the nuclear case are much larger. Both ordinate and abscissa differ by about 20 orders of magnitude between these two cases, which indicates that the size of the "glitch" corresponds to the amount of regular change occurring over roughly the same number of periods ($\sim 10^8$). The pulsar glitches are not too well understood at present but probably have to do with a sudden breaking of the solid crust on the neutron star. The nuclear glitch is much better understood as the sudden pairing of two high-j particles. In the case of this first backbend in ^{158}Er, the particles are the $i_{13/2}$ neutrons. Above I $\approx$ 14 this pair of aligned particles contributes $\sim$10 ħ along the rotation axis, but this is lost below I $\approx$ 14 when the particles suddenly couple to spin nearly zero and begin to participate in the pairing correlations. The angular momentum has to be made up by the collective rotation, which must speed up, thereby decreasing the period.

5. The Highest Spins

The previous studies have all been based on the analyses of spectra with intense resolved γ-ray lines. Below about 30 ħ where the population following heavy-ion fusion reactions

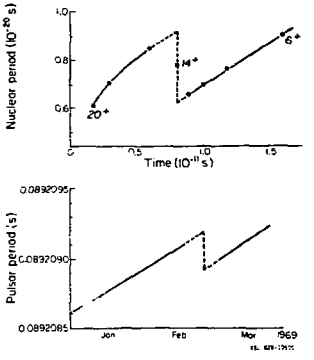

Fig. 7. Plots of rotational period vs time for the nucleus ^{158}Er (top) and the pulsar Vela (bottom).

"condenses" into a few ($\gtrsim$10) paths, one can make the kinds of detailed spectroscopic studies just described. However, above $\sim$30 $\hbar$ the population is spread over too many states and the γ-ray spectrum cannot at present be resolved. In studying the unresolved spectra from these highest spin states, the approach has necessarily been less detailed, involving shapes and moments of inertia.

5.1 Moments of Inertia

As a consequence of the interplay between collective and single particle motions, there are a variety of moments of inertia one can measure and compare with detailed nuclear model calculations. The first distinction to make is between kinematic and dynamic values. The lowest order equation for rotational motion is the usual:

$$E = \frac{\hbar^2}{2\mathcal{J}} I(I+1) \approx \frac{\hbar^2}{2\mathcal{J}} I^2 \qquad (1)$$

where the one can generally be neglected compared with I for the spins we want to consider. A moment of inertia may be defined from the first derivative of this energy with respect to spin:

$$\frac{\mathcal{J}^{(1)}}{\hbar^2} = I\left(\frac{dE}{dI}\right)^{-1} = \frac{I}{\hbar\omega} \quad , \qquad (2)$$

where $\mathcal{J}^{(1)}$ is called the "kinematic" moment of inertia because it has to do with the motion of the system--the ratio of angular momentum to angular frequency. It is also apparent that the second derivative leads to a definition:

$$\frac{\mathcal{J}^{(2)}}{\hbar^2} = \left(\frac{d^2E}{dI^2}\right)^{-1} = \frac{dI}{\hbar d\omega} \quad , \qquad (3)$$

where $\mathcal{J}^{(2)}$ is called the "dynamic" moment of inertia since it has to do with the way the system will respond to a force. If there is only the kinetic energy term as given in Eqn. 1, these are equal; but, in general, when there are additional I-dependent terms in the Hamiltonian these two moments of inertia will differ. In the present case, the Coriolis force perturbs the internal nuclear structure, giving rise, in lowest order, to an $(I\cdot j)$ term, so that $\mathcal{J}^{(1)} \neq \mathcal{J}^{(2)}$. This situation is not uncommon in other branches of physics. The arguments carry over into translational motion, where $p^2/2m$ is analogous to $I^2/2\mathcal{J}$,

and additional momentum-dependent terms in the Hamiltonian give rise to two observed masses. Bohr and Mottelson have pointed out[15] that an electron moving in a crystal lattice is a close analog, where the kinematic mass determines the level density and related statistical mechanical properties; whereas the response of the electron to an external force depends on a different, dynamic mass.

These two moments of inertia can be defined in principle for any sequence of states desired, but certain ones occur rather naturally in the decay processes. So long as the particle configuration is frozen, so that one is confined to a band, the appropriate moments of inertia are $\mathcal{J}^{(1)}_{band}$ and $\mathcal{J}^{(2)}_{band}$. If there is no perturbation (alignment, shape change, etc.) of the internal structure along this band, these correspond to "collective" values. In general, however, a single decay pathway involves a sequence of bands having different alignments. Then the overall variation of spin with frequency is different and defines "effective" moments of inertia $\mathcal{J}^{(1)}_{eff}$ and $\mathcal{J}^{(2)}_{eff}$. This $\mathcal{J}^{(2)}_{eff}$ is a slightly different moment of inertia than has been previously defined, but seems to be an appropriate one, both experimentally and theoretically. It is defined for any frequency and in regions of backbends contains contributions from both bands, giving rise to very high values. There are several reasons for preferring this $\mathcal{J}^{(2)}_{eff}$: 1) it is easy to measure experimentally as will be shown; 2) it can be measured with high resolution (small ω intervals) giving more detailed information; 3) its integral gives the usual $\mathcal{J}^{(1)}_{eff}$; and 4) the mathematical relationships we want to use require an $\mathcal{J}^{(2)}$ that is the <u>total</u> spin change in a frequency interval. The last point has to do with separating the spin increment ΔI into a part within the band ΔI_b (mostly collective) and an alignment Δi. Defining $\mathcal{J}^{(2)}_{eff}$ as the <u>total</u> spin change, $\Delta I/\Delta\omega$, leads to:

$$\frac{\Delta i}{\Delta I} = 1 - \frac{\mathcal{J}^{(2)}_{band}}{\mathcal{J}^{(2)}_{eff}} \qquad (4)$$

For the unresolved spectra from the highest spin states, the population is spread over many bands in many decay sequences. Nevertheless, the average band moments of inertia can be

determined by looking for successive rotational transitions as correlations in γ-γ coincidence spectra. Similarly, the overall spin and γ-ray energies and their variations are also measurable giving the average effective moments of inertia. Thus we can obtain information about Δi in these regions.

6. Exerimental Data on Moments of Inertia

A number of studies have been made over the last 10-15 years of the unresolved γ rays emitted from the highest spin states. It has been established that there are two types of γ rays emitted: statistical ones (3 or 4) that cool the nucleus to the yrast line and "yrast-like" ones ($\gtrsim$30) that remove the angular momentum and contain most of the nuclear structure information. For some nuclei essentially all the yrast-like transitions are collective rotational ones, and for most nuclei at least those from the very highest spin states are. In addition, systematic searches for noncollective behavior (as evidenced by the existence of isomers) have given negative results, generally above $\sim$30 ħ, and in all cases surveyed above 40 ħ. Thus the methods developed to study the highest spin states center on ways to extract information from unresolved rotational sequences and use the moment of inertia concepts discussed above.

6.1. Measurement of $\mathcal{J}^{(2)}_{band}$

The γ-ray spectrum from a rotational nucleus is highly correlated in time, spatial distribution, and energy. For a perfect rotor, it is easy to show from Eqn. 1:

$$E_\gamma = 2\,\frac{dE}{dI} = \frac{\hbar^2}{2\mathcal{J}}\,(4I_i - 2) \quad , \tag{5}$$

where I_i is the initial spin. This spectrum is composed of equally spaced lines, up to some maximum energy corresponding to the decay of the state with highest angular momentum, I_{max}. One aspect of the energy correlations is that no two γ rays have the same energy. If plotted on a two-dimensional diagram of $E_\gamma^{(1)}$ vs $E_\gamma^{(2)}$, such energies give a pattern with no points along the diagonal and a series of ridges parallel to it. The width of the "valley" W along the diagonal is determined by the difference between γ-ray energies and is thus related to the band moment of inertia,

$$W = 2\,\Delta E = 4\,\frac{dE_\gamma}{dI} = 8\,\frac{d\omega}{dI} = \frac{8\hbar^2}{\mathcal{J}^{(2)}_{band}} \quad . \qquad (6)$$

The important point is that the spectrum need not be resolved to determine the valley width. All that is required is that the populated bands have somewhat similar moments of inertia at a given frequency (γ-ray energy).

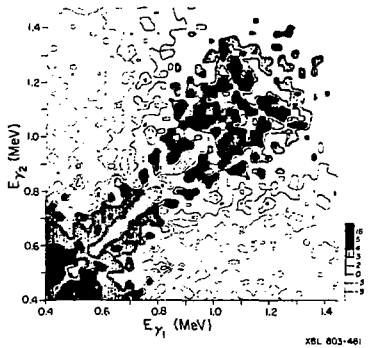

Fig. 8. Correlation spectrum from the reaction $^{124}Sn(^{40}Ar,xn)^{164-x}Er$ at 185 MeV. The data were taken on GeLi detectors and treated according to ref. 16. The plot shows contours of equal numers of correlated events, where the darker regions have more counts according to the scale at the right edge.

The data[16] in Fig. 8 come mainly from $^{159,160}Er$ nuclei formed by bombarding ^{124}Sn with ^{40}Ar at sufficient energy (185 MeV) to bring into the fused system all the angular momentum the nucleus can hold ($\sim$70 $\hbar$). The data have been "symmetrized" around the diagonal in order to improve the statistics and have an "uncorrelated" background subtracted. A valley is clear up to energies $\sim$1 MeV, and again probably from 1.1 to 1.2 MeV. Resolved lines have been seen in this case only up to $\sim$0.8 MeV. The width of the valley in both the upper and lower region is about the same and can be evaluated to give $\mathcal{J}^{(2)}_{band}/\hbar^2 \approx 50$ MeV^{-1}, around two-thirds of the rigid-body value.

In these correlation plots, the valley can be filled by irregularities in the bands, alignments, for example. These produce several transitions in the same energy region, and not only fill the valley but produce "stripes" of higher coincidence intensity at these γ-ray energies[17]. It is important to appreciate that the alignments are expected to occur in many bands at nearly the same frequency as was discussed in section 2.

These correlation techniques are potentially powerful, but not so much information has yet come from them. One problem has to do with statistics--for a pair of Ge detectors with peak-to-total areas of 0.15, the fraction of good coincidence events (full energy-full energy) is only ∿2%. Furthermore, the analysis techniques are still developing, so that one is not yet quite sure which features of the data can be fully trusted. It is my opinion that this method will only reach its full potential when the analysis methods are better understood and arrays of Compton-suppressed Ge detectors are used. Rather rapid progress is being made in both these areas.

6.2 Measurement of $\mathcal{J}^{(2)}_{eff}$

The effective moments of inertia are simpler in some respects. They involve only relating a collective γ-ray energy with a spin or measuring the number of γ rays in an energy interval. The former gives $\mathcal{J}^{(1)}_{eff}$ values and has been measured several different ways, originally by relating the maximum γ-ray energy in a spectrum with the estimated maximum spin input. Recently, however, reliable methods for obtaining $\mathcal{J}^{(2)}_{eff}$ have been developed[18] and these are much more sensitive to the nuclear structure. If desired $\mathcal{J}^{(1)}_{eff}$ can then be obtained by integration. It is apparent that in a spectrum consisting only of "stretched" electric quadrupole (I → I-2) transitions (which is known to be a good approximation in regions of rotational behavior), the number of transitions dN in a given γ-ray energy interval is just half the spin removed from that interval. If one knows the fraction of the observed population that goes through the interval, $f(E_\gamma)$, then (remembering $E_\gamma = 2\hbar\omega$):

$$\frac{H(E_\gamma)}{f(E_\gamma)} = \frac{dN}{dE_\gamma} = \frac{dI}{4\hbar\, d\omega} = \mathcal{J}^{(2)}_{eff}(\omega)/4\hbar^2 \quad . \tag{7}$$

The height of the spectrum $H(E_\gamma)$ gives directly $\mathcal{J}^{(2)}_{eff}(\omega)$. This was long recognized, but the difficulty was to find the feeding, $f(E_\gamma)$. Recently a method was developed using the spectra from two similar but slightly shifted spin distributions, whose difference is generally proportional to the feeding curve. For a constant spin shift ΔI, one can show:

$$H(E_\gamma) - H_\Delta(E_\gamma) = -\Delta I \frac{df(E_\gamma)}{dE_\gamma} \quad , \tag{8}$$

so that:

$$f(E_\gamma) = \int_{E_\gamma}^{\infty} \frac{df(E_\gamma)}{dE_\gamma}\, dE_\gamma \Big/ \int_{0}^{\infty} \frac{df(E_\gamma)}{dE_\gamma}\, dE_\gamma \quad . \qquad (9)$$

Figure 9 shows a spectrum of ^{159,160}Er resulting from the decay of a rather broad spin distribution centered at ∿55 ħ. (This distribution is defined by selecting coincidences with a slice of the total γ-ray energy emitted by the nucleus. The total energy is detected in a large NaI crystal having an overall solid angle times efficiency of ∿0.75 of 4π.) The statistical spectrum of γ rays, whose high-energy tail is seen above ∿2 MeV, is subtracted leaving a spectrum of essentially pure collective transitions, and the $\mathcal{J}^{(2)}_{eff}$ values shown by the solid line in Fig. 10 result from correcting this for

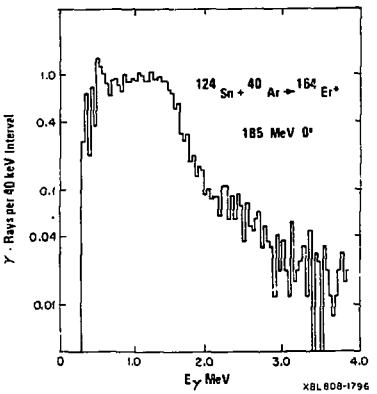

Fig. 9. Unresolved γ-ray spectrum for the indicated reaction taken with a NaI crystal and corrected for response function. The spectrum is that in coincidence with a slice of high-energy events (implying high spin) recorded in a large total-energy γ-ray detector.

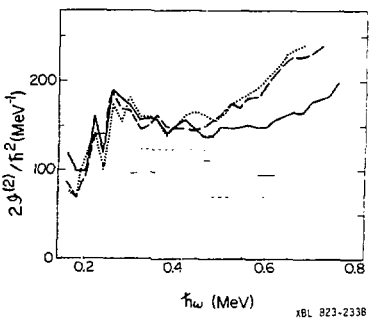

Fig. 10. $\mathcal{J}^{(2)}_{eff}$ as a function of ħω for the systems ^{124}Sn + ^{40}Ar (thick solid line), ^{126}Te + ^{40}Ar (dotted line), ^{130}Te + ^{40}Ar (thick dashed line). Also shown are some values of $\mathcal{J}^{(2)}_{band}$ for ^{124}Sn + ^{40}Ar (thin solid lines) and ^{130}Te + ^{40}Ar (thin dashed lines).

feeding[19]. Two other cases, ^{161,162}Yb and ^{165,166}Yb, are also shown in Fig. 10. The general rise at low frequencies in all these nuclei is due to the quenching of the pairing correlations, and the irregularities below $\hbar\omega \sim 0.3$ MeV result from partialy resolved individual γ-ray transitions and the known alignments (backbends), which cause several transitions to pile up at the same frequency. The band moments of inertia from the correlation data are plotted as lighter lines in the regions where they have been determined. The rise in the effective moments of inertia above frequencies of 0.5 MeV seem to be associated with a drop in the band values. This suggests that alignments are becoming more important contributors of angular momentum. The higher values for the Yb (Z = 70) nuclei compared with ^{159,160}Er (Z = 68) suggests that protons play an important role here, which is in accord with calculations that predict proton $h_{9/2}$ and $i_{13/2}$ alignments in this frequency region. Thus the present, somewhat qualitative work indicates that single particle alignment and collective rotation continue their competiton to carry the angular momentum most efficiently, though Fig. 10 suggests that single-particle motion carries a larger fraction at the highest spins. According to the general arguments of section 2, this could indicate a shift away from $\gamma \approx 0°$ into the triaxial region.

It is somewhat puzzling that these $\mathcal{J}^{(2)}_{\text{eff}}$ values do not show any detailed structure at the highest frequencies. An interesting explanation could be that there are essentially no conserved quantum numbers at these frequencies, and all bands behave similarly. But this seems unlikely, both from theoretical grounds and from the absence of highly correlated γ-ray spectra (well-developed valley-ridge structure) that should result. More likely the irregularities are washed out because the observed population is spread over many configurations and a broad temperature region. Restricting these population spreads should then reveal a wealth of detailed information. We are here at the forefront of the high-spin studies and the last conclusions (or possibilities) have been rather speculative. Nevertheless, if we cannot eventually resolve the γ-ray spectra, then I believe our understanding of this spin region will come from such studies.

7. Future Prospects

The future prospects for this field of high-spin nuclear physics look bright just now. We seem to have a good basic understanding of the physics involved, and furthermore the theoretical techniques exist to calculate most, if not all, the quantities subject to measurement. Progress in a field nearly always comes from such careful comparisons of experimental results with the expectations calculated from the best existing theories.

Experimentally the study of high-spin states has always produced innovative methods. Multiplicity filters, sum spectrometers, and correlation techniques are a few examples. At this Symposium we are going to hear the first results from yet another new method. There exist now two multiple-detector, 4π, NaI systems, one built at Oak Ridge with 72 detectors and the other at Heidelberg with 162 detectors. These instruments measure nearly all the γ rays emitted in an event and thus give, event by event, the total γ-ray energy and multiplicity, as well as the individual γ-ray energies and angular distributions. It is really hard to imagine what such information will tell us about the γ-ray cascades from the highest spin states. I will mention just one possibility that seems to me both the most obvious and the most exciting result we might hope for. A simultaneous measurement of both multiplicity and total γ-ray energy enables one to localize a region of the (E,I) plane from which the deexciting γ rays can be isolated. In Fig. 11 I have

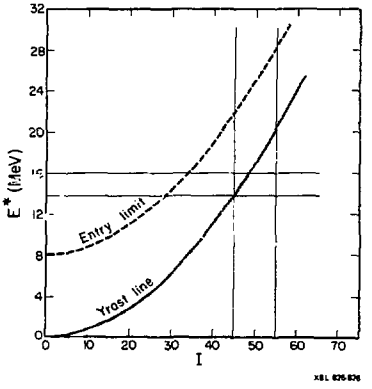

Fig. 11. A region of the E vs I plane is shown for a nucleus around A = 160, where the region decaying mainly by γ rays is indicated (between the yrast line and the entry limit), as is the region (shaded) that can be localized by the 4π NaI balls.

shown the region delimited by 20% FWHM in multiplicity and 15% FWHM in total energy (something like that expected). While this is not such a small region, it can be located in such a way as to isolate rather small regions of population--for example, along the yrast line as indicated. One or two Ge detectors placed inside the 4π balls under these conditions might be able to resolve the coincident γ-ray spectrum. Such a possibility would revolutionize our study of the highest spin states, and bring us to the level of detailed spectroscopy described in section 3 for the spin region below $\sim$30 $\hbar$.

These NaI detector systems are not the only hope in this field, however. The development of Compton-suppressed Ge detectors has proceeded rapidly in the last few years, particularly at Copenhagen and Daresbury. We at Berkeley have opted to build a system of 21 such Ge detectors in close proximity to an approximately 4π ball made out of bismuth germanate. A drawing of this system is shown in Fig. 12. While our 4π ball will have somewhat lower resolution than the existing 4π NaI balls, we hope to compensate with the power of the Ge array, which will take Compton-suppressed quadrupole coincidences at a rate comparable to that at which most existing Ge arrays take double coincidences. If the high resolution in the (E,I) plane of the NaI balls should fail to produce resolved spectra from the highest spin states, we feel there is hope that such an instrument might. In any case, it is ideally suited for a wide variety of nuclear spectroscopic studies. I am confident

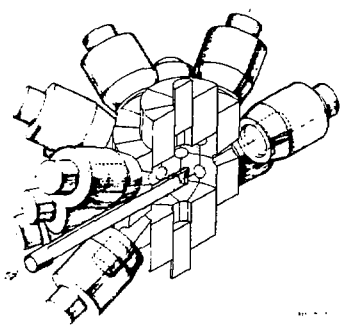

Fig. 12. A sketch of the detector system under construction at Berkeley, which consists of an inner $\sim 4\pi$ ball made of 44 elements of bismuth germanate, and an array of 21 Compton-suppressed Ge detectors outside this ball.

that these 4π systems will teach us many things about high-spin states--not only in the next session of this Symposium, but also over the coming years.

This work was supported by the Director, Office of Energy Research, Division of Nuclear Physics of the Office of High Energy and Nuclear Physics of the U.S. Department of Energy under Contract DE-AC03-76SF00098.

References

1. S. Cohen, F. Plasil, and W.J. Swiatecki, Ann. Phys. 82, 557 (1974)
2. A. Bohr and B.R. Mottelson, Mat. Fys. Medd. Dan. Vid. Selsk., 30, no. 2 (1955)
3. A. Bohr and B.R. Mottelson, Nuclear Structure, vol. 2. p. 80, 1975, Benjamin, Reading, Mass.
4. C.G. Andersson, R. Bengtsson, T. Bengtsson, J. Krumlinde, G. Leander, K. Neergaard, P. Olanders, J.A. Pinston, I. Ragnarsson, Z. Szymanski, and S. Aberg, Physica Scripta 24, 226 (1981)
5. A. Bohr, Mat. Fys. Medd. Dan. Vid. Selsk., 26, no. 14 (1952)
6. A. Johnson, H. Ryde, and J. Sztarkier, Phys. Lett. 34B, 605 (1971)
7. C. Baktash, E. der Mateosian, O.C. Kistner, and A.W. Sunyar, Phys. Rev. Lett. 42, 637 (1979)
8. A. Pakkanen, Y.H. Chung, P.J. Daly, S.R. Faber, H. Helppi, J. Wilson, P. Chowdhury, T.C. Khoo, I. Ahmad, J. Borggreen, Z.W. Grabowski, and D.C. Radford, Phys. Rev. Lett. 48, 1530 (1982)
9. O. Häusser, H.-E. Mahnke, J.F. Sharpey-Schafer, M.C. Swanson, P. Taras, D. Ward, H.R. Andrews, and T.K. Alexander, Phys. Rev. Lett. 44, 132 (1980)
10. B. Hass, H.R. Andrews, O. Häusser, D. Horn, J.F. Sharpey-Schafer, P. Taras, W. Trautmann, D. Ward, T.L. Khoo, and R.K. Smither, Phys. Lett. B84, 178 (1979)
11. B. Herskind, J. de Physique 41, C10-106, 1980
12. J. Burde, E.L. Dines, S. Shih, R.M. Diamond, J.E. Draper, K.H. Lindenberger, C. Schuck, and F.S. Stephens, Phys. Rev. Lett. 48, 530 (1982)
13. I. Hamamoto, Nordita preprint 81/28, 1981

14. J.D. Garrett and J.J. Gaardhøje, XIV Masurian Summer School on Nuclear Physics, Mikolajki, Poland, 1980
15. A. Bohr and B.R. Mottelson, Physica Scripta 24, 71 (1981)
16. M.A. Deleplanque, F.S. Stephens, O. Andersen, C. Ellegaard, J.D. Garrett, B. Herskind, D. Fossan, M. Neiman, C. Roulet, D.C. Hillis, H. Kluge, R.M. Diamond, and R.S. Simon, Phys. Rev. Lett. 45, 172 (1980)
17. C. Ellegaard, M.A. Deleplanque, O. Andersen, B. Herskind, F.S. Stephens, R.M. Diamond, H. Kluge, C. Schuck, S. Shih, and J.E. Draper, Phys. Rev. Lett. 48, 670 (1982)
18. R.S. Simons, M.V. Banaschik, R.M. Diamond, J.O. Newton, and F.S. Stephens, Nucl. Phys. A290, 253 (1977)
19. M.A. Deleplanque, H.J. Körner, H. Kluge, A.O. Macchiavelli, N. Bendjaballah, R.M. Diamond, and F.S. Stephens, submitted to Phys. Rev. Lett.